Dual Surface Sliding Mode Controller of Torque Tracking for 2-DOF Robotic Arm Driven by Electrohydraulic Servo System

Jian Zhang, Lie Yu, Jing Tang and Lei Ding

***Abstract*—The purpose of this paper is to present a torque tracking control which uses dual surface sliding mode controller (DSSMC) to provide better control performance for two degree-of-freedom robotic arm. The desired torques to drive the robotic arm is not given to be a constant or sinusoidal signal but automatically computed based on the Lagrange equation. The robotic arm consists of two segments including the upper arm and back arm which are actuated by two sets of electrohydraulic servo systems (EHSS). The DSSMC strategy is designed using two sliding surfaces and and the variable structure control laws to realize the automatic torque tracking. Compared with the PID controller and the original sliding mode controller, the DSSMC can obviously reduce the overshoot of torque tracking control and greatly improve the accuracy of torque tracking.**

***Index Terms*—Torque tracking control, dual surface sliding mode controller, two degree-of-freedom robotic arm, electrohydraulic servo systems, Lagrange equation.**

I. Introduction

At present, approximately 77% of the stroke population suffers from the impairment of the upper limb as many tasks require the cooperative use of both hands [1]. To assist the patients with stroke, rehabilitation robots have been used as therapy aids to improve their movement performance. Studies have proved that rehabilitation robots oriented repetitive movements can enhance muscular strength and movement coordination on these patients [2].

Generally, the selected actuators for this system are classified as pneumatic muscles, motors and electrohydraulic servo systems (EHSS). Many applications of pneumatic muscles and motors have been made to control humanoid robot [3]-[5]. In this paper, the realization of two degrees of freedom (2-DOF) robot rehabilitation system is made by using two sets of EHSS to accomplish high fast response and high tracking accuracy [6].

However, it is difficult to build the dynamic of EHSS because some model uncertainties exist such as the parametric disturbances and structural uncertainties. Specifically, the parametric disturbances mainly include effective bulk modulus, flow pressure coefficient and viscous damping coefficient, while the structural uncertainties consist of the relationship between input current and output flow, fluid compressibility, deadband due to the internal leakage and external load [7].

For most of the robotic arm systems, control strategies can be classified as position control, velocity control and force/torque control based on the desired objective types [8]-[9]. When position control strategy and velocity control strategies are used to control the robotic arm systems, the motion is passive as the movement coordination is previously planed. On the contrary, the robotic arm can move automatically under the force/torque control strategies because the desired force/torque can be obtained through computation methods [1].

As to force/torque tracking control strategies, the controller selection will directly affect the system performance. Generally, PID controller is most widely used due to its simple control structure, ease of design and low cost [10]. However, the PID controller is completely independent of the mathematical model of control systems, and possesses two main drawbacks such as requiring preliminary offline learning and big overshoot [11]-[12]. As a result, it is hard for PID controller to provide exact control for nonlinear and complex systems (i.e., EHSS). To overcome these drawbacks, sliding mode control (SMC) strategy is used to promote the system control performance. Specifically, SMC is achieved through switching the controller structure, including control law or control parameters, according to the degree of deviation from system status to the sliding mode, with the result that the system runs in accordance with the law provided by the sliding mode [13]-[14]. Because its sliding mode has the invariance of system parameter changes and external disturbances, and the control algorithm is more robust and relatively simple, the SMC strategy has been widely used in robot control, vehicle control and other areas [15].

In this paper, we present a 2-DOF robotic arm system which is actuated by two sets of EHSS for both the upper arm and back arm. The dynamic modeling of the EHSS and 2-DOF robotic arm is built based on the Newton equation and fluid equation. The desired torques to drive the robotic arm are computed through the Lagrange equation. Then, dual surface sliding mode controller (DSSMC) strategy for 2-DOF robotic arm is designed using the method of dual sliding surfaces design and variable structure control to realize the automatic torque tracking. Simulation results show that the

Manuscript received May 1st, 2017. This work was supported by the National Natural Science Foundation of China under Grant No. 41374148 and Educational Commission of Hubei Province of China under Grant No. Q20111306.

Jian Zhang is now with College of Computer Science, Yangtze University, JingZhou, China. (e-mail: zhangjian0716@126.com).

Lie Yu is with the School of Electronic and Electrical Engineering, Wuhan Textile University, Wuhan, China. (Corresponding author to provide phone: +86 18607155647; e-mail: lyu@wtu.edu.cn).

Jing Tang is with the School of Information and Engineering, Wuhan University of Technology, WuHan, China. (e-mail:18732463@qq.com)

Lei Ding is with the School of Information and Engineering, Wuhan University of Technology, WuHan, China. (e-mail: 398487325@qq.com)

robotic arm can move automatically, and the proposed method can obviously reduce the overshoot of torque tracking control and greatly improve the accuracy of torque tracking.

II. Modeling of EHSS and 2-DOF robotic arm

In this section, the modeling of EHSS and robotic arm has been built. This analysis utilizes the dynamic equation to show the process of EHSS driving the robotic arm. The EHSS is the same system reported by Yao *et al* [16]-[17]. The schematic diagram of 2-DOF robotic arm is drafted in Fig. 1. The robotic arm consists of two parts including a upper arm and a back arm. Two sets of EHSS are severally mounted on the mechanical frame to drive the robotic upper arm and back arm. The pump actuated by the motor feeds EHSS with oil stored in the tank. It is assumed that the supply pressure P_s keeps constant. Through the motor, the spool motion controls the oil flow from the pump. Depending on the desired control strategy, the robotic arm is driven appropriately by the bidirectional hydraulic cylinder. In actual experiments, an encoder sensor is mounted inside the robotic joints to measure the angular position which is the input signal of this study.

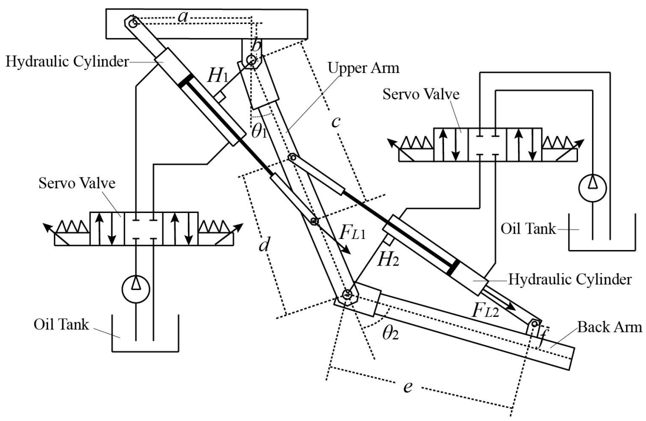

Fig. 1. Schematic Diagram of the EHSS and 2-DoF robotic arm

As pictured in Fig. 1, two sets of EHSS provide the force\torque to actuate the robotic upper arm and back arm. For EHSS, the driving torque T can be calculated as:

$$T_L = \begin{bmatrix} T_{L1} \\ T_{L2} \end{bmatrix} = \begin{bmatrix} F_{L1}H_1 \\ F_{L2}H_2 \end{bmatrix} \tag{1}$$

where T_{L1} and F_{L1} are the driving force and torque for the robotic upper arm, respectively. T_{L2} and F_{L2} are the driving force for the robotic back arm, respectively. H_1 and H_2 are the arm of force for the robotic upper arm and back arm, respectively. Due to the system geometry, the H_1 and H_2 can be computed as

$$\begin{cases} H_1 = \dfrac{c\sqrt{a^2+b^2}\sin(\theta_1+\frac{\pi}{2}+\arctan\frac{b}{a})}{\sqrt{a^2+b^2+c^2-2c\sqrt{a^2+b^2}\cos(\theta_1+\frac{\pi}{2}+\arctan\frac{b}{a})}} \\ H_2 = \dfrac{d\sqrt{e^2+f^2}\sin(\pi-\theta_1-\theta_2-\arctan\frac{f}{e})}{\sqrt{d^2+e^2+f^2-2d\sqrt{e^2+f^2}\cos(\pi-\theta_1-\theta_2-\arctan\frac{f}{e})}} \end{cases} \tag{2}$$

where a, b, c, d, e and f are the geometry lengths as pictured in Fig. 1. θ_1 and θ_2 are the angular positions of the robotic upper arm and back arm. Due to the complexity of EHSS, the F_{L1} and F_{L2} can not be directed computed, but their derivatives can be modeled using the flow equations, which is presented as follows.

$$\begin{cases} F_{L1} = P_{11}A_{p1} - P_{12}A_{p2} \\ F_{L2} = P_{21}A_{p1} - P_{22}A_{p2} \end{cases} \tag{3}$$

where P_{11} and P_{12} are the head-side pressure of hydraulic for the robotic upper and back arms, respectively; P_{21} and P_{22} are the rod-side pressure of hydraulic for the robotic upper and back arms, respectively; A_{p1} is the head-side area; A_{p2} is the rod-side area. In Eq. (3), the A_{p1} and A_{P2} can be calculated by the following formulas when the bore diameter D_1 and the rod diameter D_2 of the hydraulic are obtained.

$$\begin{cases} A_{p1} = \dfrac{\pi D_1^2}{4} \\ A_{p2} = \dfrac{\pi(D_1^2 - D_2^2)}{4} \end{cases} \tag{4}$$

However, as the the rod diameter D_2 is even less than the bore diameter D_1, the Eq. (4) can be rewritten as

$$A_{p2} = \frac{\pi(D_1^2 - D_2^2)}{4} \approx \frac{\pi D_1^2}{4} = A_{p1} \tag{5}$$

Substituting the Eq. (5) into Eq. (3) , the actual force driven by the hydraulics can be described as

$$\begin{cases} F_{L1} = (P_{11} - P_{12})A_{p1} \\ F_{L2} = (P_{21} - P_{22})A_{p1} \end{cases} \tag{6}$$

In this paper, the external and internal leakage of the hydraulic are neglected such that the pressure dynamics in both actuator chambers can be stated as

$$\begin{cases} \dot{P}_{11} = \dfrac{\beta}{V_{11}}(-A_{p1}v_{p1} - C_t P_{L1} + Q_{11}) \\ \dot{P}_{12} = \dfrac{\beta}{V_{12}}(A_{p1}v_{p1} + C_t P_{L1} - Q_{12}) \\ \dot{P}_{21} = \dfrac{\beta}{V_{21}}(-A_{p1}v_{p2} - C_t P_{L2} + Q_{21}) \\ \dot{P}_{22} = \dfrac{\beta}{V_{22}}(A_{p1}v_{p2} + C_t P_{L2} - Q_{22}) \end{cases} \tag{7}$$

where β is the effective bulk modulus in the chambers; $V_{11}=V_0+A_{p1}x_{p1}$, $V_{12}=V_0-A_{p1}x_{p1}$, $V_{12}=V_0+A_{p2}x_{p2}$ and $V_{12}=V_0-A_{p2}x_{p2}$ are the control volumes of the actuator chambers. V_0 is chamber volume such that at $x_{p1}=0$, $V_{11}=V_{12}=V_0$ or $x_{p1}=0$, $V_{21}=V_{22}=V_0$; x_{p1} and x_{p2} are the load displacement of the robotic upper and back arms, respectively; C_t is the coefficient of the total internal leakage of the actuator due to the pressure; $P_{L1}=P_{11}-P_{12}$ and $P_{L2}=P_{21}-P_{22}$ are the load pressure of the dynamic actuator of the robotic upper and back arms, respectively; Q_{11} and Q_{21} are the supplied flow rate to the forward chamber, and Q_{12} and Q_{22} are the return flow rate of the return chamber. Q_{11}, Q_{12}, Q_{21} and Q_{22} are related to the spool valve displacement of the servo-valve x_v.

$$\begin{cases} Q_{11} = C_d w\sqrt{\dfrac{2}{\rho}}x_{v1}[s(x_{v1})\sqrt{P_s - P_{11}} + s(-x_{v1})\sqrt{P_{11} - P_r}] \\ Q_{12} = C_d w\sqrt{\dfrac{2}{\rho}}x_{v1}[s(x_{v1})\sqrt{P_{12} - P_r} + s(-x_{v1})\sqrt{P_s - P_{12}}] \\ Q_{21} = C_d w\sqrt{\dfrac{2}{\rho}}x_{v2}[s(x_{v2})\sqrt{P_s - P_{21}} + s(-x_{v2})\sqrt{P_{21} - P_r}] \\ Q_{22} = C_d w\sqrt{\dfrac{2}{\rho}}x_{v2}[s(x_{v2})\sqrt{P_{22} - P_r} + s(-x_{v2})\sqrt{P_s - P_{22}}] \end{cases} \tag{8}$$

where C_d is the discharge coefficient, w is the spool valve area gradient, ρ is the density of hydraulic oil, x_{v1} and x_{v2} are the spool valve displacement of the servo valve mounted in robotic upper and back arms. P_s is the supply pressure of the fluid, and P_r is the return pressure. In addition, $s(x_v)$ is defined as

$$s(x_v) = \begin{cases} 1, & x_v \geq 0 \\ 0, & x_v < 0 \end{cases} \tag{9}$$

The spool position is related to the input current by the first order differential equation, which can be described as.

$$\dot{x}_v = \frac{1}{\tau}(k_s i - x_v) \tag{10}$$

where k_s is the gain of input electrical to the spool position, τ is the mechanical time constant of the spool, and i is the current input into the servo valve.

However, the x_{p1}, v_{p1}, x_{p2} and v_{p2} can be calculated based on the system geometric model.

$$\begin{cases} x_{p1} = \sqrt{a^2 + b^2 + c^2 + 2c\sqrt{a^2+b^2}\sin(\arctan(\frac{b}{a}) + \theta_1)} - L_0 - x_{p0} \\ v_{p1} = \dfrac{2c\sqrt{a^2+b^2}\cos(\arctan(\frac{b}{a}) + \theta_1)}{\sqrt{a^2 + b^2 + c^2 + 2c\sqrt{a^2+b^2}\sin(\arctan(\frac{b}{a}) + \theta_1)}} \\ x_{p2} = \sqrt{d^2 + e^2 + f^2 - 2d\sqrt{e^2+f^2}\cos(\arctan(\frac{f}{e}) + \theta_2)} - L_0 - x_{p0} \\ v_{p2} = \dfrac{2d\sqrt{e^2+f^2}\sin(\arctan(\frac{f}{e}) + \theta_2)}{\sqrt{d^2 + e^2 + f^2 - 2d\sqrt{e^2+f^2}\cos(\arctan(\frac{f}{e}) + \theta_2)}} \end{cases} \tag{11}$$

where L_0 is the cylinder dead length and x_{p0} is the piston position when the volumes are equal on both cylinder sides. In practical working conditions, P_{11}, P_{12}, P_{21} and P_{22} are both bounded by P_s and P_r, which can be presented that $0<P_r<P_{11}<P_s$, $0<P_r<P_{12}<P_s$, $0<P_r<P_{21}<P_s$ and $0<P_r<P_{22}<P_s$. For simulation, P_L should be bounded by P_s such that $-P_s<P_{L1}<P_s$ and $-P_s<P_{L2}<P_s$.

III. Deriving and solving 2-DOF dynamic equation

The controller design of this system is to track the desired torques in the movement of robotic arm. In this study, the desired torques are conducted through the Lagrange equation which can be described as

$$T_d = \frac{d}{dt}\frac{\partial E}{\partial \dot{q}} - \frac{\partial E}{\partial q} \tag{12}$$

where T_d is the torque desired by robotic arm, E is the total energy of the whole system and q is the joint rotary angle. In addition, the Eq. (12) can also be rewritten as

$$T_d = M(q)\ddot{q} + C(q,\dot{q}) + G(q) \tag{13}$$

where M is the inertia torque caused by angular acceleration, C is the torque caused by centripetal force and G is the torque caused by gravity. For this system, the T_d, M, C and G in Eq. (13) can be presented as follows.

$$T_d = \begin{bmatrix} T_{d1} \\ T_{d2} \end{bmatrix} \quad q = \begin{bmatrix} \theta_1 \\ \theta_2 \end{bmatrix} \quad M = \begin{bmatrix} M_{11} & M_{12} \\ M_{21} & M_{22} \end{bmatrix}$$

$$G = \begin{bmatrix} G_1 \\ G_2 \end{bmatrix} \quad C = \begin{bmatrix} C_{11} & C_{12} \\ C_{21} & C_{22} \end{bmatrix}\begin{bmatrix} \dot{q}_1^2 \\ \dot{q}_2^2 \end{bmatrix} + \begin{bmatrix} C_{13} & C_{14} \\ C_{23} & C_{24} \end{bmatrix}\begin{bmatrix} \dot{q}_1\dot{q}_2 \\ \dot{q}_2\dot{q}_1 \end{bmatrix} \tag{14}$$

where T_{d1} and T_{d2} are the actuated torques imposed by EHSS on robotic upper and back arms, respectively. θ_1 and θ_2 are the angular position of robotic upper and back arms, respectively. The elements of matrix M, C and G can be expressed as follows.

$$\begin{aligned} &M_{11} = I_1 + I_2 + m_1 L_{g1}^2 + m_2(L_1^2 + L_{g2}^2) + 2m_2 L_1 L_{g2}\cos(\theta_2) \\ &M_{12} = M_{21} = I_2 + m_2 L_{g2}^2 + m_2 L_1 L_{g2}\cos(\theta_2) \\ &M_{22} = I_2 + m_2 L_{g2}^2 \\ &C_{11} = C_{22} = C_{23} = C_{24} = 0 \\ &C_{12} = C_{13} = C_{14} = -m_2 L_1 L_{g2}\cos(\theta_2) \\ &C_{21} = m_2 L_1 L_{g2}\cos(\theta_2) \\ &G_1 = m_2 g L_{g2}\sin(\theta_1 + \theta_2) + m_1 g L_{g1}\sin(\theta_1) + m_2 g L_1 \sin(\theta_1) \\ &G_2 = m_2 g L_{g2}\sin(\theta_1 + \theta_2) \end{aligned} \tag{15}$$

where m_1 is the upper arm mass, m_2 is the back arm mass, L_1 is the upper arm length, L_2 is the back arm length, L_{g1} is the the position of the center of the upper arm mass, L_{g2} is the the position of the center of the back arm mass, I_1 is the upper arm inertia and I_2 is the back arm inertia.

The computation of the desired torque T_d needs the angular velocity (i.e., $\dot{q}$) and angular acceleration (i.e., $\ddot{q}$). In actual experiments, the $\dot{q}$ and $\ddot{q}$ are obtained using the encoder sensor and accelerometer. For simulation, the differential of joint rotary angel (i.e., q) would give the $\dot{q}$ and $\ddot{q}$, as q is the input signal of this system. However, this paper uses the forward dynamic to conduct the $\ddot{q}$ which calculates the $\dot{q}$ in integral way. When the actual torque T_L is imposed on the robotic arm, the movement of the robotic arm would generate the angular position, velocity and acceleration. This can be described as

$$\ddot{q} = M^{-1}(q)(T_L - C(q,\dot{q}) - G(q)) \tag{16}$$

The q, C and G are given in Eq. (10), and M^{-1} is the inverse matrix of M Which is written as

$$M^{-1} = \begin{bmatrix} H_{R11} & H_{R12} \\ H_{R21} & H_{R22} \end{bmatrix} \tag{17}$$

The elements of matrix M^{-1} can be expressed as follows.

$$H_{note} = 4I_1 m_2 L_2^2 + 16 I_1 I_2 + 4m_2^2 L_1^2 L_2^2 + 16 m_2 L_1^2 I_2 + m_1 L_1^2 m_2 L_2^2 + 4m_1 L_1^2 I_2 - 4m_2^2 L_1^2 L_2^2 (\cos(\theta_2))^2$$

$$H_{R11} = \frac{4(m_2 L_2^2 + 4I_2)}{H_{note}}$$

$$H_{R12} = \frac{-4(4I_2 + 2m_2 L_1 L_2 \cos(\theta_2) + m_2 L_2^2)}{H_{note}}$$

$$H_{R21} = \frac{-4(4I_2 + 2m_2 L_1 L_2 \cos(\theta_2) + m_2 L_2^2)}{H_{note}}$$

$$H_{R22} = \frac{4(4\mathrm{I}_1 + 4\mathrm{m}_2\mathrm{L}_1^2 + 4\mathrm{m}_2\mathrm{L}_1\mathrm{L}_2\cos(\theta_2) + \mathrm{m}_2\mathrm{L}_2^2 + \mathrm{m}_1\mathrm{L}_1^2 + 4\mathrm{I}_2)}{H_{note}}$$

(18)

The $\ddot{\theta}_1$ and $\ddot{\theta}_2$ can be obtained using the forward dynamic equation in Eq. (12). However, $\dot{\theta}_1$ and $\dot{\theta}_2$ should also be acquired. In this study, the $\dot{\theta}_1$ and $\dot{\theta}_2$ are computed using the integral way, which can be written as:

$$\begin{cases} \dot{\theta}_1(t+1) = \dot{\theta}_1(t) + \ddot{\theta}_1(t)dt \\ \dot{\theta}_2(t+1) = \dot{\theta}_2(t) + \ddot{\theta}_2(t)dt \end{cases} \tag{19}$$

Finally, the calculated angular velocities and accelerations are used in Eq. (9) to deduce the desired torques. When the actual and desired torques are obtained, the controller design can be made to implement the control strategy.

IV. Controller design.

The aim of the controller is to evaluate the torque tracking performance of EHSS such that the desired and actual torques should be obtained before controller design. In this paper, the positions θ_1 and θ_2 are the rotary angles of the robotic shoulder and elbow joints, which is presented in Fig. 2. However, it is impossible to sense the the robot joints' movements. To make it understandable, the visible changes of robot joints' movement is captured, which is showed in Fig. 3. Then, the controller design can be made at a sampling frequency of f_s=1000 Hz to examine the behavior of this system.

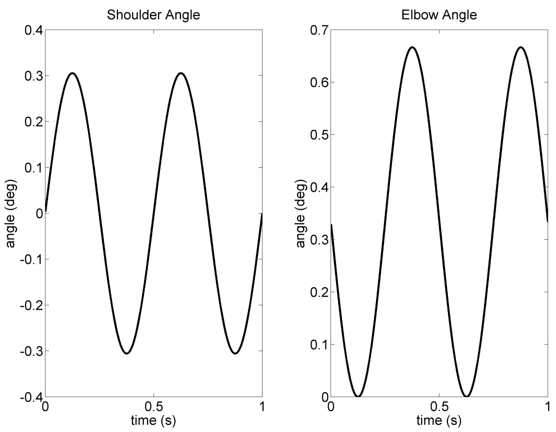

Fig. 2. The moving angles of robotic joints

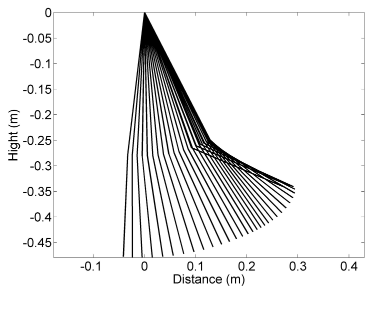

Fig. 3. The visible movements of robotic joints

A. Design of the PID controller

Generally, the conventional PID controller is most widely used due to its simple control structure, ease of design and low cost. The control law of PID controller can be presented as follows.

$$i = K_p e(t) + K_i \int e(t)dt + K_d \frac{de(t)}{dt} \tag{20}$$

where K_p, K_i *and* K_d are the proportional, integral and differential gains, respectively. $e(t) = T_d(t) - T_L(t)$ is the error between the desired and actual torques of the system.

B. Design of the sliding mode controller

The system robustness can be added by using the properties of SMC. For this system, neglecting the spool dynamics, the Eq. (7) can be rewritten as

$$x_v = k_s i \tag{21}$$

Thus, from Eq. (6) and Eq. (11), $s(x_v)$=$s(i)$ can be conducted. From the Eq. (1) to Eq. (8), the system dynamic can be described in the form.

$$\begin{cases} \dot{T}_{L1} = (\frac{R_{11}}{V_{11}} + \frac{R_{22}}{V_{12}})H_1 A_{p1} \beta g_s i_1 - (\frac{1}{V_{11}} + \frac{1}{V_{12}})(\beta C_t P_{L1} + A_{p1} v_{p1}) H_1 A_{p1} \\ \dot{T}_{L2} = (\frac{R_{21}}{V_{21}} + \frac{R_{22}}{V_{22}})H_2 A_{p1} \beta g_s i_2 - (\frac{1}{V_{21}} + \frac{1}{V_{22}})(\beta C_t P_{L2} + A_{p1} v_{p2}) H_2 A_{p1} \end{cases} \tag{22}$$

where

$$g_s = k_s C_d w \sqrt{\frac{2}{\rho}}$$

$$\begin{cases} R_{11} = s(i_1)\sqrt{P_s - P_{11}} + s(-i_1)\sqrt{P_{11} - P_r} \\ R_{12} = s(i_1)\sqrt{P_{12} - P_r} + s(-i_1)\sqrt{P_s - P_{12}} \\ R_{21} = s(i_2)\sqrt{P_s - P_{21}} + s(-i_2)\sqrt{P_{21} - P_r} \\ R_{22} = s(i_2)\sqrt{P_{22} - P_r} + s(-i_2)\sqrt{P_s - P_{22}} \end{cases} \tag{23}$$

Then, the SMC strategy can be designed. First of all, the sliding surface should be defined, which is shown as follows.

$$s(t) = \begin{bmatrix} s_1(t) \\ s_2(t) \end{bmatrix} = \begin{bmatrix} T_{L1}(t) - T_{d1}(t) \\ T_{L2}(t) - T_{d2}(t) \end{bmatrix} \tag{24}$$

Thus, we define a candidate Lyapunov function as

$$V = \frac{1}{2}s^2 \tag{25}$$

In Eq. (25), V must be positive definite. If in addition, $\dot{V}$ must be negative definite, then $s(t)$ is asymptotically stable at the equilibrium $s(t)$=0. Therefore, we would like to have $V = s\dot{s} < 0$ for $s \geq 0$, where is the boundary layer [18]. From Eq. (22) and Eq. (24), it can be conducted that

$$\dot{s}(t) = \begin{bmatrix} \dot{s}_1(t) \\ \dot{s}_2(t) \end{bmatrix} = \begin{bmatrix} f_{11}i_1 + f_{12} - \dot{T}_{d1}(t) \\ f_{21}i_2 + f_{22} - \dot{T}_{d2}(t) \end{bmatrix} \tag{26}$$

where

$$\begin{cases} f_{11} = (\frac{R_{11}}{V_{11}} + \frac{R_{22}}{V_{12}})H_1 A_{p1} \beta g_s \\ f_{12} = -(\frac{1}{V_{11}} + \frac{1}{V_{12}})(\beta C_t P_{L1} + A_{p1} v_{p1}) H_1 A_{p1} \\ f_{21} = (\frac{R_{21}}{V_{21}} + \frac{R_{22}}{V_{22}})H_2 A_{p1} \beta g_s \\ f_{22} = -(\frac{1}{V_{21}} + \frac{1}{V_{22}})(\beta C_t P_{L2} + A_{p1} v_{p2}) H_2 A_{p1} \end{cases} \tag{27}$$

Thus, $\dot{V}$ can be described as

$$\dot{V}=s(t)\dot{s}(t)=\begin{bmatrix} s_1(t)(f_{11}i_1+f_{12}-\dot{T}_{d1}(t)) \\ s_2(t)(f_{21}i_2+f_{22}-\dot{T}_{d2}(t)) \end{bmatrix} \tag{28}$$

In order to keep the system stable, the the control law would be chosen to be like this.

$$\begin{cases} i_1(t)=-\dfrac{1}{f_{11}}(f_{12}-\dot{T}_{d1}(t)+K_1s_1(t)) \\ i_2(t)=-\dfrac{1}{f_{21}}(f_{22}-\dot{T}_{d2}(t)+K_2s_2(t)) \end{cases} \tag{29}$$

In Eq. (29), if the K_1 and K_2 are selected such that $s\dot{s}\le -s^2$, s will be converge to be the boundary layer. Therefore, K_1 and K_2 can be selected as:

$$\begin{cases} K_1=\dfrac{(1-f_{11\min})\left|f_{12}-\dot{T}_{d1}(t)\right|}{f_{11\min}} \\ K_2=\dfrac{(1-f_{21\min})\left|f_{22}-\dot{T}_{d2}(t)\right|}{f_{21\min}} \end{cases} \tag{30}$$

where $f_{11}>f_{11\min}>0$ and $f_{21}>f_{21\min}>0$.

C. Design of the dual surface sliding mode controller

The controller design for the previous section can be extended to include the spool dynamics through using the DSSMC technique. Then, the system can be defined as

$$\begin{cases} T_{L1}(t)=f_{11}x_{v1}(t)+f_{12} \\ \dot{x}_{v1}(t)=g_1i_1(t)+g_2x_{v1}(t) \\ T_{L2}(t)=f_{21}x_{v2}(t)+f_{22} \\ \dot{x}_{v2}(t)=g_1i_2(t)+g_2x_{v2}(t) \end{cases} \tag{31}$$

where $g_1=k_s/\tau$ and $g_2=-1/\tau$. Similarly, define the first sliding surface.

$$s_1(t)=\begin{bmatrix} s_{11}(t) \\ s_{12}(t) \end{bmatrix}=\begin{bmatrix} T_{L1}(t)-T_{d1}(t) \\ T_{L2}(t)-T_{d2}(t) \end{bmatrix} \tag{32}$$

where s_1 is totally different from that of the previous section. Then, differentiating s_1, it can be given that.

$$\dot{s}_1(t)=\begin{bmatrix} \dot{s}_{11}(t) \\ \dot{s}_{12}(t) \end{bmatrix}=\begin{bmatrix} f_{11}x_{v1}(t)+f_{12}-\dot{T}_{d1}(t) \\ f_{21}x_{v2}(t)+f_{22}-\dot{T}_{d2}(t) \end{bmatrix} \tag{33}$$

After that, define the second sliding surface.

$$s_2(t)=\begin{bmatrix} s_{21}(t) \\ s_{22}(t) \end{bmatrix}=\begin{bmatrix} x_{v1}(t)-x_{vd1}(t) \\ x_{v2}(t)-x_{vd2}(t) \end{bmatrix} \tag{34}$$

where x_{vd} is the synthetic input to make s_1 asymptotically stable about zero. In order to meet this demand, the x_{vd} is chosen as

$$\begin{cases} x_{vd1}(t)=-\dfrac{1}{f_{11}}(s_{11}(t)+f_{12}-\dot{T}_{d1}(t)) \\ x_{vd2}(t)=-\dfrac{1}{f_{21}}(s_{21}(t)+f_{22}-\dot{T}_{d2}(t)) \end{cases} \tag{35}$$

where

$$\operatorname{sgn}(x)=\begin{cases} 1, & x>0 \\ 0, & x=0 \\ -1, & x<0 \end{cases} \tag{36}$$

Thus, we define a candidate Lyapunov function as

$$V=\frac{1}{2}s_1^2+\frac{1}{2}s_2^2 \tag{37}$$

Then, $\dot{V}$ can be described as

$$\begin{aligned} \dot{V}&=s_1\dot{s}_1+s_2\dot{s}_2 \\ &=\begin{bmatrix} s_{11}(f_{11}x_{v1}+f_{12}-\dot{T}_{d1}) \\ s_{12}(f_{21}x_{v2}+f_{22}-\dot{T}_{d2}) \end{bmatrix}+\begin{bmatrix} s_{21}(g_1i_1+g_2x_{v1}-x_{vd1}) \\ s_{22}(g_1i_2+g_2x_{v2}-x_{vd2}) \end{bmatrix} \\ &=\begin{bmatrix} s_{11}(f_{11}(s_{21}+x_{vd1})+f_{12}-\dot{T}_{d1}) \\ s_{12}(f_{21}(s_{22}+x_{vd2})+f_{22}-\dot{T}_{d2}) \end{bmatrix} \\ &+\begin{bmatrix} s_{21}(g_1i_1+g_2x_{v1}-x_{vd1}) \\ s_{22}(g_1i_2+g_2x_{v2}-x_{vd2}) \end{bmatrix} \\ &=\begin{bmatrix} -s_{11}^2+s_{21}(f_{11}s_{11}+g_1i_1+g_2x_{v1}-\dot{x}_{vd1}) \\ -s_{12}^2+s_{22}(f_{21}s_{12}+g_1i_2+g_2x_{v2}-\dot{x}_{vd2}) \end{bmatrix}<0 \end{aligned} \tag{38}$$

In order to keep the system stable, the the control law would be chosen to be like this.

$$\begin{cases} i_1(t)=\dfrac{1}{f_{11}}(\text{-}\gamma_1s_{21}(t)-f_{11}s_{11}(t)-g_2x_{v1}(t)+\dot{x}_{vd1}(t)-\eta_1s_{21}(t)) \\ i_2(t)=\dfrac{1}{f_{21}}(\text{-}\gamma_2s_{22}(t)-f_{21}s_{12}(t)-g_2x_{v2}(t)+\dot{x}_{vd2}(t)-\eta_2s_{22}(t)) \end{cases} \tag{39}$$

In Eq. (39), if the γ_1, γ_2, η_1 and η_2 are selected such that $\dot{V}\le 0$, s_1 and s_2 will be converge to be the boundary layer. Therefore, γ_1, γ_2, η_1 and η_2 can be selected as:

$$\begin{cases} \eta_1=\dfrac{(g_{1\max}-1)\left|x_{vd1}-g_2\right|}{g_{1\max}} \\ \eta_2=\dfrac{(g_{1\max}-1)\left|x_{vd2}-g_2\right|}{g_{1\max}} \\ \gamma_1>\dfrac{f_{11}(1-g_1)}{2} \\ \gamma_2>\dfrac{f_{21}(1-g_1)}{2} \end{cases} \tag{40}$$

where $g_{1\max}>g_1>0$.

V. SIMULATION RESULTS

A. Selection of system parameters.

In order to show the control effect of this system, the EHSS and the 2-DOF robotic arm are simulated with the following nominal parameters: m_1=0.5kg, m_2=0.6kg, L_1=0.25m, L_2=0.3m, L_{g1}=0.14m, L_{g2}=0.18m, I_1=0.0071$kg{\cdot}m^2$, I_2=0.043$kg{\cdot}m^2$, D_1=0.07m, D_2=0.2×10^{-4} m^2, a=0.14m, b=0.06m, c=0.26 m, d=0.17 m, e=0.06 m, f=0.28 m, P_s=2×10^6 Pa, P_r=0.5×10^5 Pa, L_0=0.1m, x_{p0}=0.08m, β=2×10^7 Pa, V_0=1.15×10^{-4} m^3, C_t=8×10^{-12} $m^5N^{-1}s^{-1}$, C_d=0.61, w=9.6×10^{-3} m^2, ρ=830kg/m^3, ks=0.015 and τ=0.0015.

As to the parameter selection of the PID controller, the gains K_p, K_i and K_d are chosen using Ziegler-Nichols method. Then, optimum gains of K_{p1}=0.1, K_{i1}=4 and K_{d1}=1 are acquired for the PID controller to track the torque of the robotic upper arm. In addition, the gains for the PID controller to take the best tracking tracking of the robotic back arm are selected that k_{p2}=0.3, k_{i2}=1 and k_{d2}=1.3.

For the SMC, the parameters for the control law are chosen that $f_{11\min}$=0.95 and $f_{21\min}$=0.85. Similarly, the the parameters for the DSSMC are selected that $g_{1\min}$=11, $g_{2\min}$=15, γ_1=10, and γ_2=18.

B. Control effect.

The system simulation is accomplished through Matlab in the light of the introduced EHSS model and 2-DOF robotic arm. The control blocks for the PID controller, SMC controller and DSSMC controller are shown fro Fig. 4 to Fig. 6.

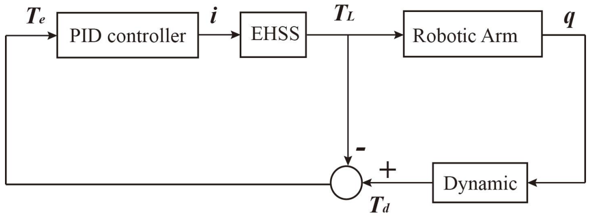

Fig. 4. Control block of PID controller

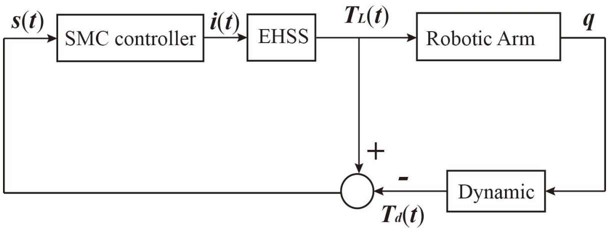

Fig. 5. Control block of SMC controller

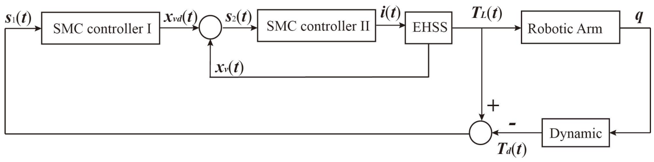

Fig. 6. Control block of DSMC controller

On the other hand, mean absolute error (MAE) is used to evaluate the control effect, and the MAE is defined in the following.

$$MAE = \frac{1}{n}\sum_{i=1}^{n}\left|T_d(i) - T_L(i)\right| \tag{41}$$

Then, the tracking lag and mean absolute error (MAE) are utilized to judge the control effect, which is described in Fig. 7 and Fig. 8. In addition, the Fig. 7 demonstrates the control effect for the robotic upper arm, while the control effect of the robotic back arm is pictured in Fig. 8.

As shown in Fig. 7, the SMC and DSSMC obtains the same tracking lag (13ms), which is less than PID controller (lag=18ms). However, the DSSMC acquires the least MAE value (1.37N.m) than PID controller (1.41N.m) and SMC (1.57N.m).

As to the control effect for robotic back arm, the DSSMC provides the least tracking lag (12ms) and MAE value (0.56N.m) than PID controller (lag=12ms and MAE=0.57N.m) and SMC (lag=14ms and MAE=0.62N.m). The results show that the DSSMC leads to the reduction in the control lag and MAE, which is shown in Table I. In addition, the DSSMC can promote the system performance for robotic arm. Due to the DSSMC, the EHSS can achieve better displacement control for spool valve, which is shown in Fig. 9. When the spool valve displacement is controlled exactly, the actuated torque can be generated precisely such that the EHSS can drive the robotic arm better as expected.

TABLE I
COMPARISON OF CONTROL EFFECT

Controller Types	Control Lag (ms)	MAE (N.m)
PID	18	1.57
SMC	13	1.41
DSSMC	13	1.37

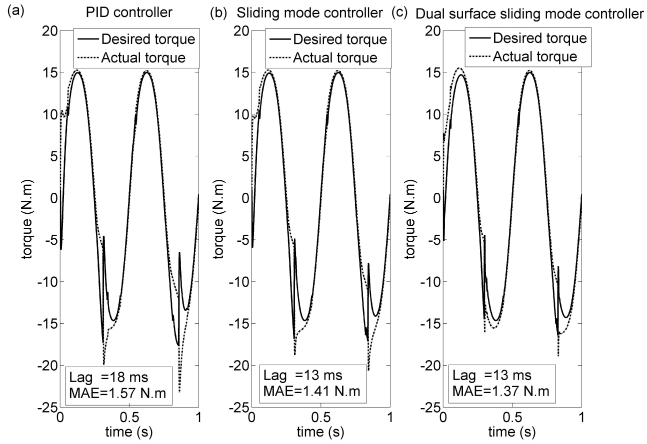

Fig. 7. Control effect for robotic upper arm using three types of controllers: (a) PID controller, (b) Sliding mode controller, (c) Dual surface sliding mode controller.

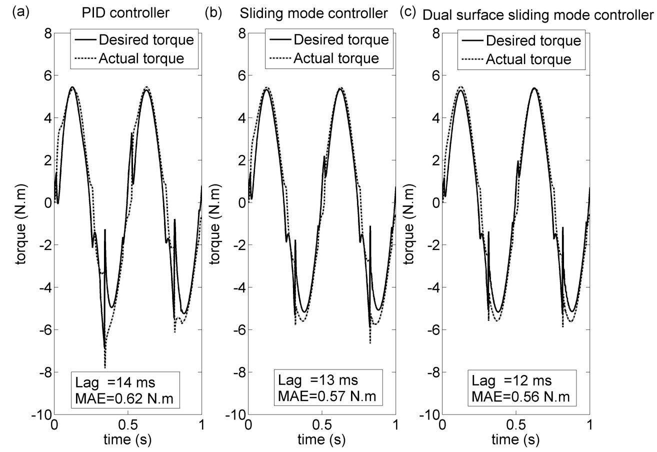

Fig. 8. Control effect for robotic back arm using three types of controllers: (a) PID controller, (b) Sliding mode controller, (c) Dual surface sliding mode controller.

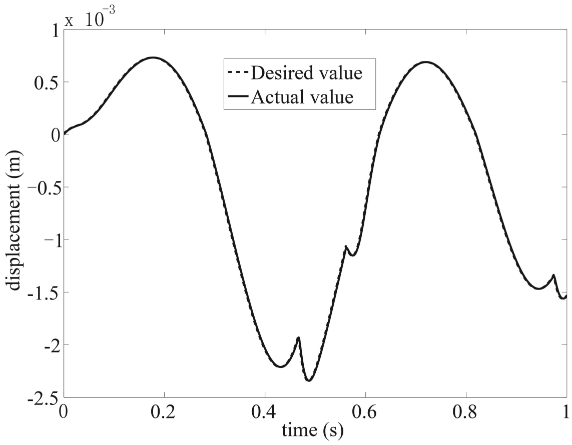

Fig. 9. The control effect of spool valve displacement.

The errors between the desired torques and the actual driving toques are shown in Fig. 10 and Fig 11, where the magnitudes of the errors using the DSSMC is the least compared with the other controllers. The MAE values show that using DSSMC results in reduction of the driving torque errors.

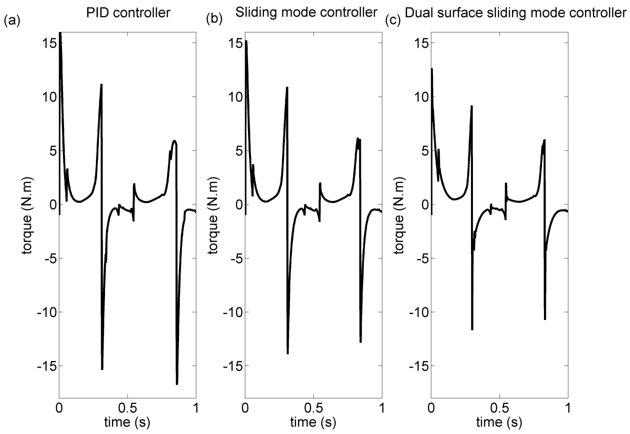

Fig. 10. Control errors for robotic upper arm using three types of controllers: (a) PID controller, (b) Sliding mode controller, (c) Dual surface sliding mode controller.

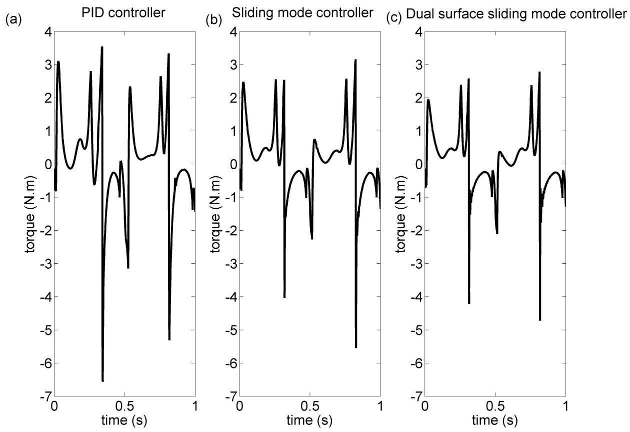

Fig. 11. Control errors for robotic back arm using three types of controllers: (a) PID controller, (b) Sliding mode controller, (c) Dual surface sliding mode controller.

The simulation results show that the DSSMC leads to the reduction of tracking lag and MAE value. For DSSMC, the spool valve displacement is controlled, while not for PID controller and SMC controller. As the spool valve controls the flow rate of hydraulic oil, the pressure from the valve is generated. The control of spool valve displacement can give the precise force to actuate the hydraulic cylinder. As a result, the DSSMC can result in the reduction of tracking lag and MAE value. Additionally, the comparative results also suggest that the DSSMC gives better performance for 2-DOF robotic arm.

VI. Conclusion

A mathematical model of 2-DOF robotic arm actuated by EHSS is successfully developed, simulated and tested at MATLAB. The approach to mimic the robotic upper and back arm segments is original through torque tracking control strategy. The robotic arm can provide the desired torque automatically with the movement of the robotic because the desired torque is computed through the Lagrange equation with the knowledge of robotic joint masses, lengths, inertia and angles. Moreover, DSSMC is developed to offer more exact control effect in term of torque tracking. In order to obtain comparative and convincing results, two types of other controllers (i.e., PID controller and original SMC) are used. Simulation results shows that the DSSMC acquires less MAE and less tracking lag in term of position control strategy.

Acknowledgment

This work is supported by the National Natural Science Foundation of China under Grant No. 41374148 and Educational Commission of Hubei Province of China under Grant No. B2015445. We are also grateful to the referee for their helpful comments and suggestions of the reviewers, which have improved the presentation.

References

[1] P. R. Culmer,et al, “A Control Strategy for Upper Limb Robotic Rehabilitation With a Dual Robot System”, *IEEE/ASME Transactions on Mechatronics.*, vol. 15, no. 4, pp. 575-585, 2010.

[2] A. M. Amin, A. A. Rahim and Y. L. Cheng, “Adaptive controller algorithm for 2-DOF humanoid robot arm”, *2nd international conference on system integrated intelligence: Challenges for product and production engineering.*, pp. 765-774, 2014.

[3] J. Fleszar and E. A. Mendrela, “Twin-armature rotary-linear induction motor”, *IEEE Proc. B.*, vol. 130, no. 3, pp. 186 – 192, 1983

[4] K. J. Meessen, J. H. Paulides and E. A. Lomonova, “Analysis of a novel magnetization pattern for 2-DoF rotary-linear actuators”, *IEEE Trans. Magn.*, vol. 48, no. 11, pp. 3867-3870, 2012.

[5] E. A. Mendrela and E. Gierczak, “Double winding rotary linear induction motor”, *IEEE Trans. Energy Convers.,* vol. 2, no. 1, pp. 47-54, 1987.

[6] J. C. Gao and P. D. Wu, “A fuzzy neural network controller in the electrohydraulic position control system”, *IEEE international conference on intelligent systems.*, vol. 1, pp. 58-63, 1997.

[7] C. L. Hwang, “Neural-Network-Based Variable Structure Control of Electrohydraulic Servosystems Subject to huge uncertainties without persistent excitation”, *IEEE/ASME Transactions on mechatronics.*, vol. 4, no. 1, pp. 50-59, 1999.

[8] T. L. Chern and Y. C. Wu, “An optimal variable structure control with integral compensation for electrohydraulic position servo control systems”, *IEEE transaction on industrial electronics.*, vol. 39, no. 5, pp.460-463, 1992.

[9] S. Tafazoli, C.W. Silva and P. D. Lawrence, “Tracking control of an elechydraulic manipulator in the presence of friction”, *IEEE Transactions on control system technology.*, vol. 6, no. 3, pp. 401-411, 1998.

[10] M. S. Zaky, “A self-tuning PI controller for the speed control of electrical motor drives”, *Electric Power Systems Research.*, pp. 293 – 303, 2015.

[11] Jie-Sheng Wang, and Shu-Xia Li, "PID Decoupling Controller Design for Electroslag Remelting Process Using Cuckoo Search Algorithm with Self-tuning Dynamic Searching Mechanism," Engineering Letters, vol. 25, no.2, pp125-133, 2017.

[12] Zhongda Tian, Xianwen Gao, and Dehua Wang, "The Application Research of Fuzzy Control with Self-tuning of Scaling Factor in the Energy Saving Control System of Pumping Unit," Engineering Letters, vol. 24, no.2, pp187-194, 2016.

[13] J. M. Yang and J. H. Kim, “Sliding mode control for trajectory tracking of nonholonomic wheeled mobile robots”, *IEEE Transactions on Robotics and Automatio*n., vol. 15, no. 3, pp: 578-587, 1999.

[14] K. D. Young, V. I. Utkin and U.Ozguner, “A control engineer’s guide to sliding mode Control”. *IEEE Transactions on Control Systems Technology.*, vol.7, no. 3, pp: 328-342, 1999.

[15] G. Chen, W. G. Zhang and X. N. Zhang, “Speed Tracking Control of a Vehicle Robot Driver System Using Multiple Sliding Surface Control Schemes”, *International Journal of Advanced Robotic Systems.*, vol. 10, pp:1-9, 2013.

[16] J. Y. Yao, Z. X. Jiao and S. S. Han, “Friction compensation for low velocity control of hydraulic flight motion simulator: A simple adaptive robust approach”, *Chinese Journal of Aeronautics*., vol. 26, no. 3, pp. 814-822, 2013.

[17] J. Y. Yao, Z. X. Jiao and B. YAO, “Robust Control for Static Loading of Electro-hydraulic Load Simulator with Friction Compensation”, *Chinese Journal of Aeronautics*., vol. 25, no. 6, pp. 954-962, 2012.

[18] C. R. Jean-Louis, “Control of a lower extremity exoskeleton for human performance amplification”, working paper, University of California, Berkeley, 2003.